

Graphene Oxide Hierarchical Patterns for the Derivation of Electrophysiologically Functional Neuron-like Cells from Human Neural Stem Cells

Kisuk Yang,^{†,‡,⊥} Jaehong Lee,^{§,⊥} Jong Seung Lee,[†] Dayeong Kim,[§] Gyeong-Eon Chang,[†] Jungmok Seo,[§] Eunji Cheong,[†] Taeyoon Lee,^{*,§} and Seung-Woo Cho^{*,†}

[†]Department of Biotechnology, Yonsei University, Seoul 120-749, Republic of Korea

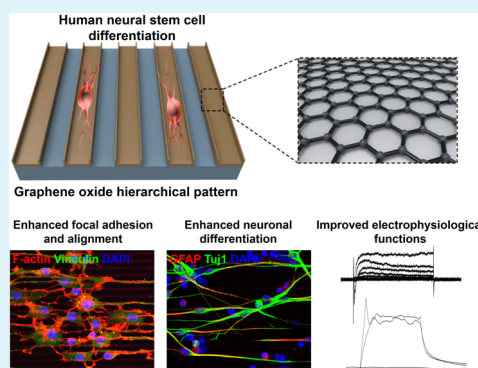
[‡]Department of Biomaterials Science and Engineering, Yonsei University, Seoul 120-749, Republic of Korea

[§]School of Electrical and Electronic Engineering, Yonsei University, Seoul 120-749, Republic of Korea

S Supporting Information

ABSTRACT: Graphene has shown great potential for biomedical engineering applications due to its electrical conductivity, mechanical strength, flexibility, and biocompatibility. Topographical cues of culture substrates or tissue-engineering scaffolds regulate the behaviors and fate of stem cells. In this study, we developed a graphene oxide (GO)-based patterned substrate (GPS) with hierarchical structures capable of generating synergistic topographical stimulation to enhance integrin clustering, focal adhesion, and neuronal differentiation in human neural stem cells (hNSCs). The hierarchical structures of the GPS were composed of microgrooves (groove size: 5, 10, and 20 μm), ridges (height: 100–200 nm), and nanoroughness surfaces (height: ~ 10 nm). hNSCs grown on the GPS exhibited highly elongated, aligned neurite extension along the ridge of the GPS and focal adhesion development that was enhanced compared to that of cells grown on GO-free flat substrates and GO substrates without the hierarchical structures. In particular, GPS with a groove width of 5 μm was found to be the most effective in activating focal adhesion signaling, such as the phosphorylation of focal adhesion kinase and paxillin, thereby improving neuronal lineage commitment. More importantly, electrophysiologically functional neuron-like cells exhibiting sodium channel currents and action potentials could be derived from hNSCs differentiated on the GPS even in the absence of any of the chemical agents typically required for neurogenesis. Our study demonstrates that GPS could be an effective culture platform for the generation of functional neuron-like cells from hNSCs, providing potent therapeutics for treating neurodegenerative diseases and neuronal disorders.

KEYWORDS: human neural stem cell, graphene oxide pattern, hierarchical topography, focal adhesion, neuronal differentiation, electrophysiology



1. INTRODUCTION

Graphene, a carbon-based material fully packed into a honeycomb lattice,¹ has attracted a massive amount of interest over a wide range of fields such as electronics, nanotechnology, energy harvesting, and biological engineering due to its electrical conductivity, high mechanical strength, flexibility, and biocompatibility.^{2,3} In particular, many studies have verified the utility of graphene-based materials for biomedical engineering applications such as antiviral⁴ and bactericidal nanomaterials,⁵ disease diagnosis,^{6,7} drug delivery,^{8–10} and tissue engineering.^{11–13} Stem cell engineering using the graphene or chemically exfoliated graphene oxide (GO) has been investigated as one such potential biomedical application due to its physicochemical and electrical properties that allow control of cellular behaviors (e.g., adhesion, proliferation, differentiation, polarization, and paracrine secretion) and biocompatibility.^{14–18} Previous studies have reported enhanced

adhesion, proliferation, and differentiation of mesenchymal stem cells on graphene or GO substrates based on their chemical properties and patterning.^{12,19} In addition, it has been demonstrated that the differentiation of neural stem cells (NSCs), which are sensitive to electrical signals, could be promoted on the surface of graphene or GO substrates due to their electrical properties.²⁰

The topographical features of culture substrates or tissue-engineering scaffolds can provide biophysical stimulation that regulates the self-renewal and differentiation of stem cells.^{21–24} Specific topographies of the surfaces have been found to induce morphological changes and cellular alignment in stem cells, evoking a series of cellular events of integrin clustering,

Received: February 13, 2016

Accepted: June 20, 2016

assembly of focal adhesion proteins (focal adhesion kinase (FAK), vinculin, and paxillin), cytoskeleton reorganization, and nuclear deformation.^{25–27} Therefore, topographical stimulation can activate mechanotransduction pathways for transcriptional regulation, which ultimately lead to alterations in the expression profiles of genes associated with self-renewal, proliferation, and differentiation of stem cells, thereby inducing phenotypic changes in stem cells and affecting stem cell functions.^{24,26,28} Several studies have indeed reported axonal alignment and enhanced neuronal differentiation of NSCs by graphene-based topographical structures.^{17,20,29}

In this study, we developed a highly effective graphene-based culture platform to provide hierarchical topographical cues that can substantially enhance focal adhesion signals of human NSCs (hNSCs) and derive functional neuronal phenotypes from hNSCs. GO-based patterned substrates (GPS) with these hierarchical topographies were fabricated to contain both microscale-grooves and nanoscale-roughness/ridges to generate synergistic topographical stimulation, enabling enhanced neuronal differentiation of hNSCs by simultaneously providing integrin clustering sites and guiding cytoskeleton extension. We previously demonstrated the effectiveness of hierarchically patterned substrates made of block copolymer for significantly enhancing the differentiation of hNSCs to neuronal lineage.²⁶ In the present study, we verified the hypothesis that GPS with hierarchical topographies of specific dimensions has the ability to promote enhanced integrin clustering, focal adhesion signals, and the subsequent neuronal differentiation of hNSCs compared to that of flat SiO₂ substrates or GO substrates without hierarchical topographies. The derivation of electrophysiologically functional neuron-like cells from hNSCs differentiated on the GPS was demonstrated using patch-clamp analysis, indicating that the GPS could be an effective culture platform that can produce functional stem cell therapeutics with enhanced therapeutic efficacy to address neurodegenerative diseases and neuronal disorders.

2. MATERIALS AND METHODS

2.1. Fabrication of the GO-Based Patterned Substrate (GPS).

For the fabrication of GPS with various sizes of grooves on the SiO₂ substrates, the substrates were first cleaned with successive sonication in acetone, isopropyl alcohol, and deionized (DI) water. Anisotropic line patterns with various groove sizes were prepared using a conventional photolithography process with a negative photoresist (DNR-L300–30, Dongjin SemiChem Co. Ltd., Seoul, Korea) on the SiO₂ substrates. Before GO was coated on the samples, the surfaces of the samples were functionalized with a self-assembled monolayer of positively charged 3-aminopropyltriethoxysilane (APTES) by being immersed in a 4 mM solution of APTES dissolved in DI water for 30 min at room temperature. The samples were then heated at 110 °C for 5 min. The functionalized samples were immersed into a GO solution (Graphene Supermarket, Reading, MA, United States) at a concentration of 0.6 mg/mL for 1 h and then annealed at 110 °C. After 5 min, the samples were dried under nitrogen flow, and the photoresist was lifted by weak sonication in acetone.

2.2. Surface Characterization. Surface morphologies were examined using a JEOL JSM-7001F field emission scanning electron microscope (FE-SEM, JEOL Ltd., Tokyo, Japan) and a Park System XE-100 atomic force microscope (AFM, Park Systems, Suwon, Korea). The Raman spectrum of GO was obtained using a HORIBA Lab Ram ARAMIS Raman spectrometer (HORIBA, Ltd., Kyoto, Japan). A Nd:YAG laser (532 nm) was used as a light source, and the excitation light was focused on the sample using a 100× microscope objective and a diffraction grating of 600 gr/mm.

2.3. Adsorption of Fibronectin. The substrates were coated with fibronectin (FN) (R&D Systems, Minneapolis, MN, United States) to facilitate hNSC adhesion. For FN adsorption, the substrates were immersed into an FN solution (10 mg/mL FN in phosphate-buffered saline (PBS)) for 2 h at 37 °C. To quantify the adsorption efficiency of FN on the substrates, the solution containing the unattached FN was retrieved immediately after completing a coating process. The concentration of FN in the retrieved solution was determined using a BCA assay kit (Thermo Scientific, Waltham, MA, United States) according to the manufacturer's instruction.

2.4. hNSC Culture. The seeding and culture conditions for the expansion of undifferentiated hNSCs are described in our previous reports.^{30,31} For differentiation experiments, hNSCs were seeded onto the substrates (seeding density: 3.0 × 10⁵ cells/mL), and spontaneous differentiation of hNSCs on the substrates was induced by maintaining the cells under culture conditions without the mitogenic factors fibroblast growth factor (bFGF) and leukemia inhibitory factor (LIF).²⁶ hNSCs at passages 10–15 were used for the experiments.

2.5. Immunocytochemistry. All procedures for immunocytochemical staining of hNSCs cultured on the substrates (fixation, permeabilization, blocking, and primary/secondary antibody incubation) were performed according to our previous protocols.^{26,32} The primary antibodies used for the staining are as follows: mouse monoclonal antineuronal class III β -tubulin (Tuj1) (1:100; Millipore, Temecula, CA, United States), rabbit polyclonal antimicrotubule-associated protein 2 (MAP2) (1:200; Santa Cruz Biotechnology, Santa Cruz, CA, United States), rabbit polyclonal antigial fibrillary acidic protein (GFAP) (1:200; Millipore), rabbit polyclonal antineuronal cell adhesion molecule (NCAM) (1:200; Millipore), mouse monoclonal antipaxillin (1:200; Millipore), and mouse monoclonal anti- β 1 integrin (1:200; Millipore). The following secondary antibodies were used for immunofluorescent staining: Alexa Fluor-488 goat antimouse IgG (1:500) and Alexa Fluor-594 donkey antirabbit IgG (1:500) (Invitrogen, Carlsbad, CA, United States). Counterstaining of cell nuclei was performed with 4',6-diamidino-2-phenylindole (DAPI, Sigma, St. Louis, MO, United States). A confocal microscope (LSM 700, Carl Zeiss, Jena, Germany) was used to detect fluorescent signals. Neurite formation and body lengths of Tuj1-positive cells were quantified as previously described.^{26,33} To stain the focal adhesion protein (vinculin) and cytoskeleton (filamentous actin: F-actin) in hNSCs after 5 days in culture, the cells on the substrates were stained with the Actin Cytoskeleton and Focal Adhesion Staining Kit (FAK100) (Millipore) and observed under a confocal microscope (LSM 700, Carl Zeiss).³³

2.6. Quantitative Real-Time Polymerase Chain Reaction (qRT-PCR). All procedures for qRT-PCR analysis (total RNA extraction, cDNA synthesis, and PCR) were conducted as described in our previous literature.²⁶ Gene expression in hNSCs on each substrate was measured ($n = 3$ per group) using TaqMan gene expression assays (Applied Biosystems, Foster City, CA, United States) (Nestin: Hs00707120_s1, Tuj1: Hs00801390_s1, MAP2: Hs00258900_m1, GFAP: Hs00909238_g1, oligodendrocyte transcription factor 2 (Olig2): Hs00300164_s1 and FAK: Hs01056457_m1, paxillin: Hs01104424_m1, vinculin: Hs00419715_m1, and β 1 integrin: Hs00559595_m1). The comparative C_t method was applied to determine the relative expression of each target gene by normalizing the expression of the target gene to that of an endogenous reference (glyceraldehyde 3-phosphate dehydrogenase (GAPDH): Hs02758991_g1).³³

2.7. Scanning Electron Microscopy (SEM). The morphology of hNSCs on the substrates was observed by SEM. Fixation, dehydration, and drying of the samples for SEM imaging were carried out as previously described.²⁵ The dried samples mounted on an aluminum stub were sputter-coated with platinum and then imaged by FE-SEM (JEOL Ltd.).

2.8. Western Blot. All procedures for Western blot analysis (total protein extraction, gel electrophoresis, membrane transfer, blocking, and antibody incubation) were conducted using our previous protocols.^{26,34} The primary antibodies used for Western blot are as follows: rabbit polyclonal anti-FAK (pY397, 1:1000; Invitrogen),

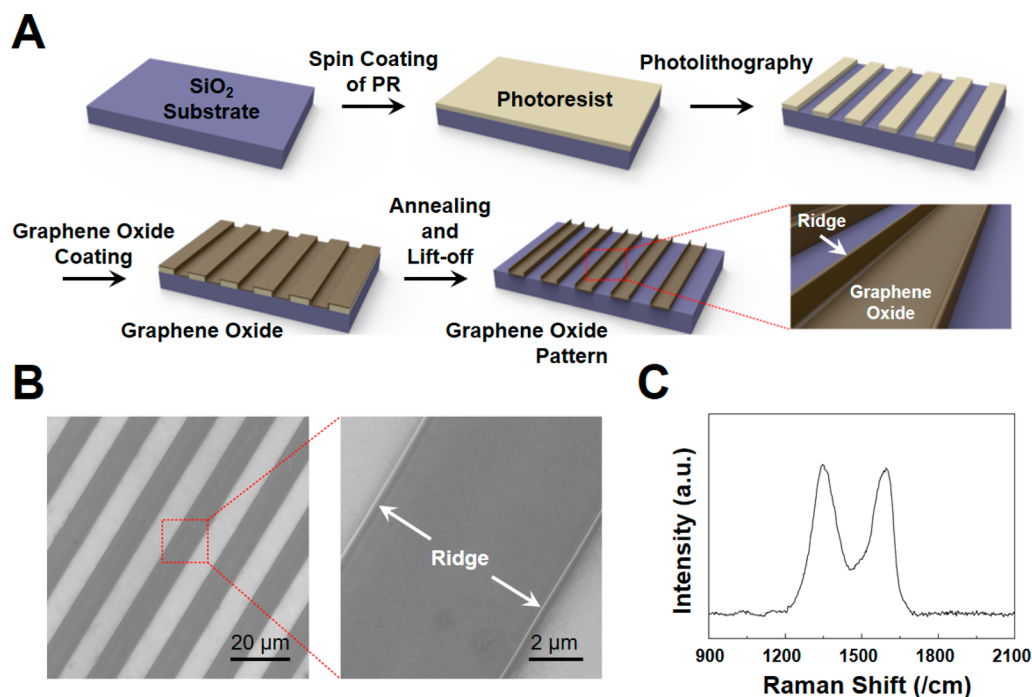


Figure 1. Preparation of GO-based patterned substrates. (A) Schematic illustration of GPS fabrication. (B) High-magnification SEM images of the GPS (groove size: 10 μm). (C) Raman spectroscopy analysis of the GPS.

rabbit polyclonal antipaxillin (pY118, 1:1000; Cell Signaling Technology, Beverly, MA, United States), and rabbit monoclonal anti- β -actin (1:2500; Cell Signaling). A Clarity Western ECL Substrate (Bio-Rad, Hercules, CA, United States) was used to detect the signal of the target proteins.

2.9. Inhibition Assay. To identify potential mechanisms of the enhancement in focal adhesion formation and differentiation of hNSCs on the GPS, inhibition assays for several cellular events were performed according to a protocol modified from our previous studies.^{25,26} Adhesion of hNSCs onto FN-coated substrates was inhibited by the treatment of anti- β 1 integrin (1:40; Millipore). To inhibit the myosin II and Rho-associated protein kinase (ROCK) pathways involved in actin organization, hNSCs were treated with 50 μM blebbistatin (Sigma) and 10 μM Y27632 (Millipore), respectively. To inhibit the mitogen-activated protein kinase/extracellular signal-regulated kinase (MEK-ERK) pathway, cells were treated with ERK1/2 inhibitor (25 μM U0126, Cell Signaling Technology). All inhibitors (anti- β 1 integrin, blebbistatin, Y27632, and U0126) were added to the culture medium when the cells were seeded onto the substrates. After one day in culture, the treated cells were immunofluorescently stained for F-actin, vinculin, Tuj1, and GFAP and observed using a confocal microscope (LSM 700). The gene expression profiles of focal adhesion proteins (FAK and vinculin) and differentiation markers (Tuj1 and GFAP) in hNSCs treated with inhibitors were examined by qRT-PCR analysis. The gene expression in the treated cells on each substrate was normalized to that in cells on the flat SiO_2 substrate with no treatment. One day after inhibitor treatments, the proliferation of hNSCs was also determined by measuring the mitochondrial activity of the cells using a 3-(4,5-dimethylthiazol-2-yl)-2,5-diphenyltetrazolium bromide (MTT) assay (Sigma) and normalizing the mitochondrial activity of cells on each substrate to that of nontreated cells on the flat substrate.

2.10. Electrophysiology. Whole-cell patch-clamping for the investigation of electrophysiological functionality of hNSCs was conducted using a protocol employed in our previous studies.^{26,30} Electrophysiological recordings of action potentials and ion channel currents from differentiated hNSCs on the GPS were carried out 5 days in the culture. To examine whether the currents and spikes were Na^+ channel specific, the cells were treated with 0.5 μM tetrodotoxin (TTX) (Sigma) for 5–10 min.

2.11. Statistical Analysis. Statistical analyses were conducted as previously described.²⁵ An unpaired Student's *t*-test for statistical analysis was performed with Sigma-Plot software (Systat Software Inc., Chicago, IL, United States). Values of *p* < 0.01 or 0.05 were considered statistically significant.

3. RESULTS AND DISCUSSION

3.1. Fabrication of GO-Based Patterned Substrates.

Here, three types of substrates with different widths of groove patterns (5, 10, and 20 μm , spacing ratio: 1) were tested to derive functional neuron-like cells from hNSCs: flat SiO_2 substrates (FS), GO-coated substrates (GS), and GO-based patterned substrates (GPS). To prepare the structures, photoresist-based line patterns with various groove widths were first fabricated on SiO_2 substrates through a conventional photolithography process (Figure 1A). We used SiO_2 for the fabrication of GO substrates because it is a widely used material for a variety of microfabrication processes with graphene, and the SiO_2 substrate has been applied as a typical template for the culture of various types of cells due to its biocompatibility.^{17,20,35} Because GO is negatively charged due to its carboxyl groups, a self-assembled monolayer of positively charged APTES was applied on the surface of the line-patterned samples before coating with GO via electrostatic interaction. To deposit GO on the surfaces of the substrates, the substrates were immersed in an aqueous GO solution for 1 h and annealed at 110 $^\circ\text{C}$ under ambient conditions. After 5 min, a GPS that exhibited nanoroughness on the GO surface as well as microsized line patterns was successfully obtained through a photoresist lift-off step. The ridges at both ends of each GO line pattern were generated by an annealing step following GO coating (Figure 1B).

The structural characteristics of the GO in the GPS were confirmed by Raman spectroscopy, which indicates the presence of a D peak (1347 cm^{-1}) and a G peak (1594 cm^{-1}) (Figure 1C). Figure 2A provides SEM and AFM images

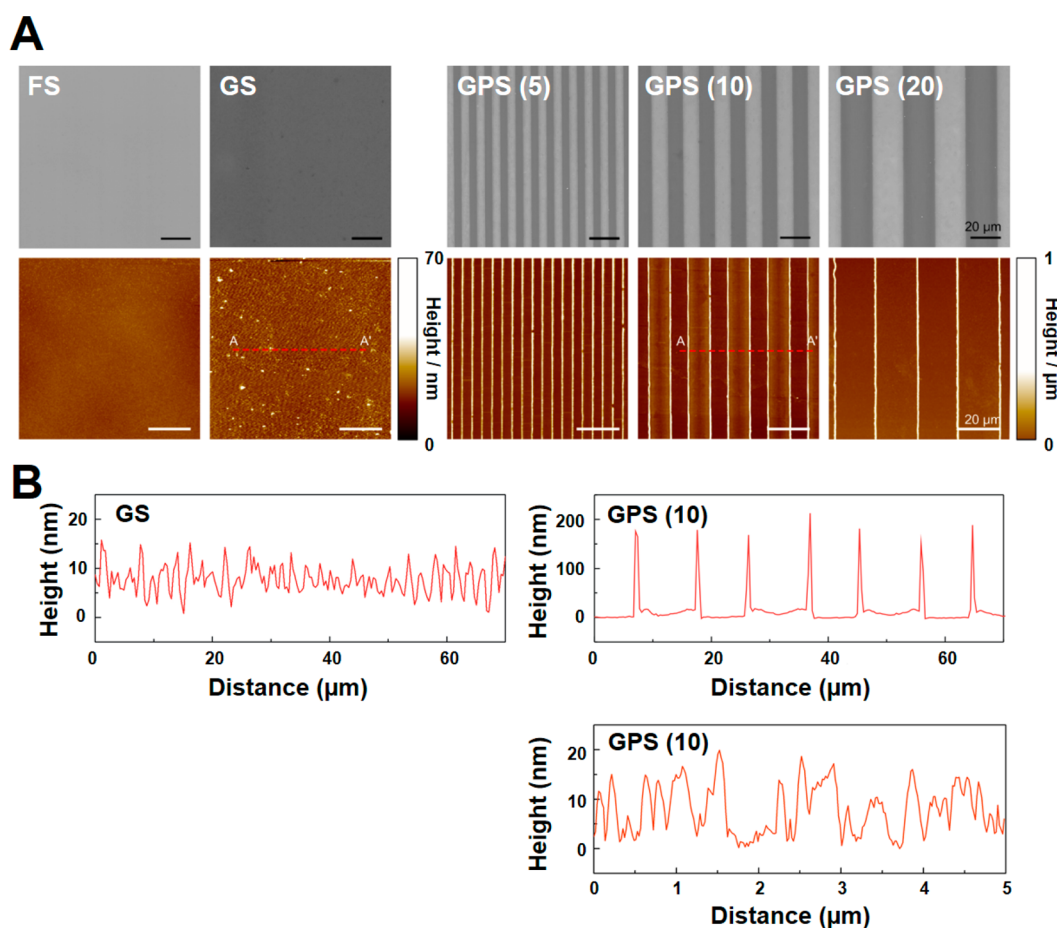


Figure 2. Surface characterization of the substrates. (A) SEM and AFM images of flat substrate, GO-coated substrate, and GO-based patterned substrates with microgroove (5, 10, and 20 μm) ridges. (B) Cross-sectional topography of GS and GPS with 10 μm microgrooves. The image of GS showed nanoroughness formed on the GO-coated substrate. Two images of GPS (10) showed the presence of nanoroughness on the groove between the ridges, indicating hierarchical patterned structures on the GPS.

showing the FS, GS, and well-defined GPS with various groove widths and the same spacing ratio of 1. Cross-sectional graphs from AFM images of the GS and GPS with 10 μm groove widths were taken along the dashed line A–A' displayed in the corresponding AFM images (Figures 2A and B). The formation of GS and GPS can be clearly verified from the cross-sectional graphs of the AFM images. The GS provided only nanoroughness with a root-mean-square (rms) value of 3.86 nm over the whole surface of the substrates, whereas the GPS exhibited a hierarchical structure of GO, including nanoroughness, micro-sized grooves, and ridges, with an average height of 179 ± 19 nm at both ends of each GO line pattern (Figure 2B). These fabricated GO-based substrates did not exhibit cytotoxicity when tested for hNSC culture, as confirmed by a Live/Dead staining assay (Supplementary Figure S1), suggesting the excellent biocompatibility of GO-based substrates.

3.2. Enhancement of Integrin Clustering, F-actin Alignment, and Focal Adhesion Formation of hNSCs by GO-Based Topography. First, we tested whether GO-based nanoscale roughness topography can efficiently induce integrin clustering and focal adhesion development in hNSCs derived from human fetal brain. The GO substrates were coated with FN to facilitate adhesion of hNSCs. FN could be efficiently deposited onto the GO substrates due to the presence of several functional groups (e.g., epoxide, carboxyl, and hydroxyl groups) in the GO for protein absorption.^{12,36}

The nanoscale roughness generated on the coated GO layers (GS group in Figure 2A) could potentially provide focal contact points that can interact with integrin molecules. Immunofluorescent staining of hNSCs for $\beta 1$ integrin interacting with FN showed strong signals, indicating clustered integrins in hNSCs cultured on GS compared with the cells on FS (Figure 3A, bottom row images) and enhancement of integrin clustering in hNSCs due to the GO-based nanoscale roughness topography. The enhancement of focal adhesion formation in hNSCs on the GS was confirmed by the increased expression of focal adhesion proteins (vinculin and paxillin) (Figure 3A, top and middle row images).

The hierarchical structures of GPS with both nanoroughness and microgroove patterns further enhanced integrin clustering and also facilitated the alignment of the cytoskeleton in hNSCs. Immunofluorescent staining of $\beta 1$ integrin revealed that integrin clustering in the hNSCs cultured on the GPS with 5 μm groove patterns was the most extensive, compared to those on other substrates (FS, GS, and GPS with 10 and 20 μm groove widths) (Figure 3A; images in the bottom row). In addition, qRT-PCR analysis of hNSCs cultured on the substrates also showed that hNSCs on the GPS with 5 μm groove patterns exhibit the most upregulated gene expression of $\beta 1$ integrin (Figure 3C). The images in the top and middle rows in Figure 3A indicate that the cytoskeleton (F-actin) of hNSCs on the FS or GS was randomly extended, whereas the

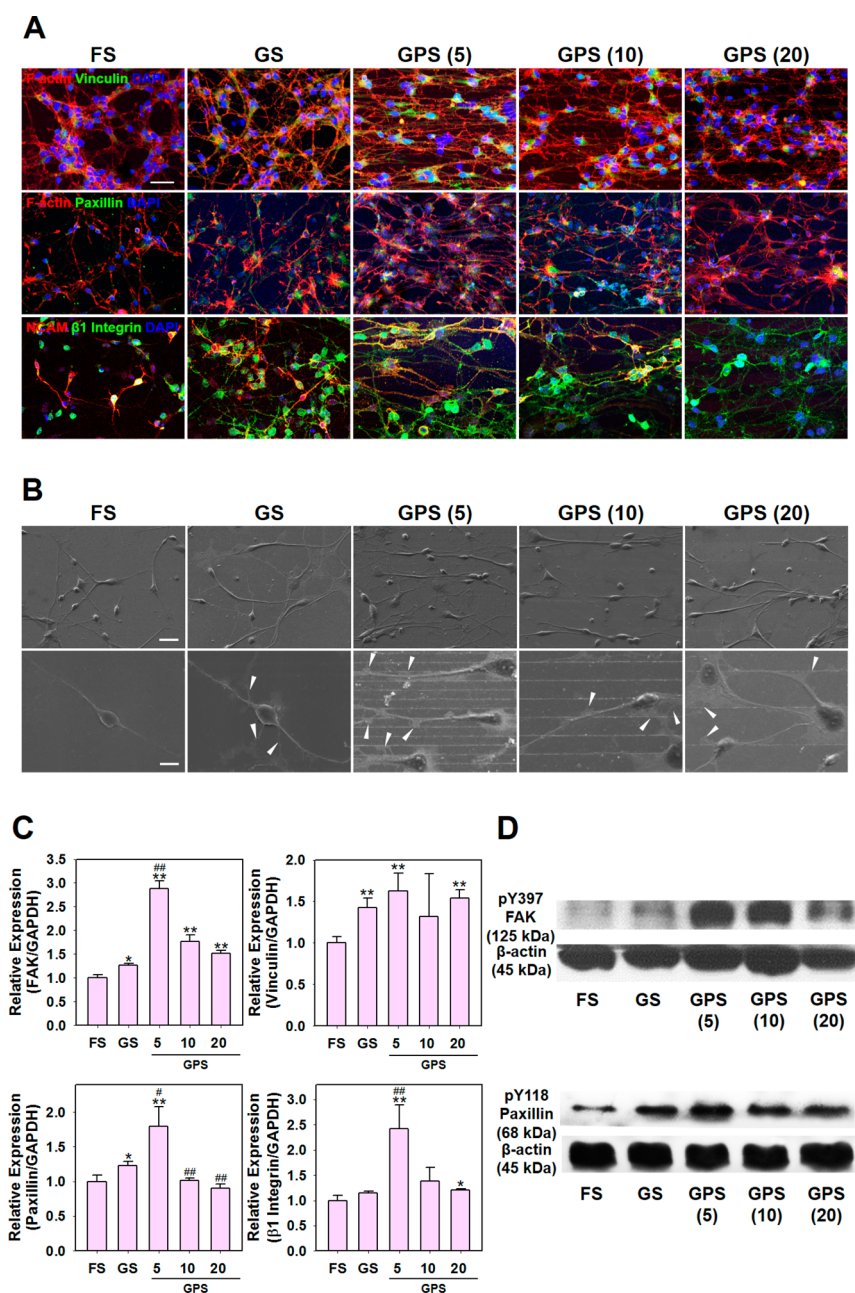


Figure 3. Focal adhesion formation and cytoskeleton alignment of hNSCs on each substrate (FS, GS, and GPS) 5 days in culture. (A) Co-staining of F-actin (cytoskeleton) and vinculin or paxillin (focal adhesion proteins) in hNSCs (scale bar = 50 μm). Co-staining of NCAM (adhesion molecule) and $\beta 1$ integrin in hNSCs. (B) SEM observation of hNSCs on the substrates (scale bars = 10 μm (top) and 20 μm (bottom)). Sprouting of neurites from cells was indicated by the white arrowheads. (C) qRT-PCR analysis for examining the gene expression of focal adhesion proteins (FAK, vinculin, and paxillin) and $\beta 1$ integrin in hNSCs grown on the substrates ($n = 3$; * $p < 0.05$, ** $p < 0.01$ versus the FS group; # $p < 0.05$, ## $p < 0.01$ versus the GS group). (D) Western blot analysis to compare the expression of phosphorylated FAK (at Y397) and paxillin (at Y118) in hNSCs cultured on each substrate.

F-actin fiber bundles of hNSCs on the GPS were highly organized, elongated, and aligned along the groove/ridge topographical features. The expression of NCAM in hNSCs was also increased on the GPS with 5 μm microgroove patterns and aligned along the groove patterned lines (Figure 3A; the images at bottom row).

GPS surfaces with hierarchical topographies significantly promoted focal adhesion formation and subsequently activated focal adhesion signaling in the hNSCs. Immunofluorescent staining for focal adhesion-associated proteins (vinculin and paxillin) (top and middle row images of Figure 3A) indicate

that focal adhesion development of hNSCs is greatly promoted on the GPS, especially on the one with a 5 μm groove width compared to that in FS and GS. Figure 3B shows the SEM images of hNSCs cultured on each substrate, indicating that the GPS with 5 μm groove patterns can provide more contact points for focal adhesion development of hNSCs and neurite sprouting from cell bodies (arrowheads) than FS or GS. qRT-PCR analysis also confirmed that the gene expression levels of focal adhesion proteins, including vinculin, paxillin, and FAK, in hNSCs cultured on the GPS with 5 μm groove patterns was the highest among all tested substrates (Figure 3C). Western blot

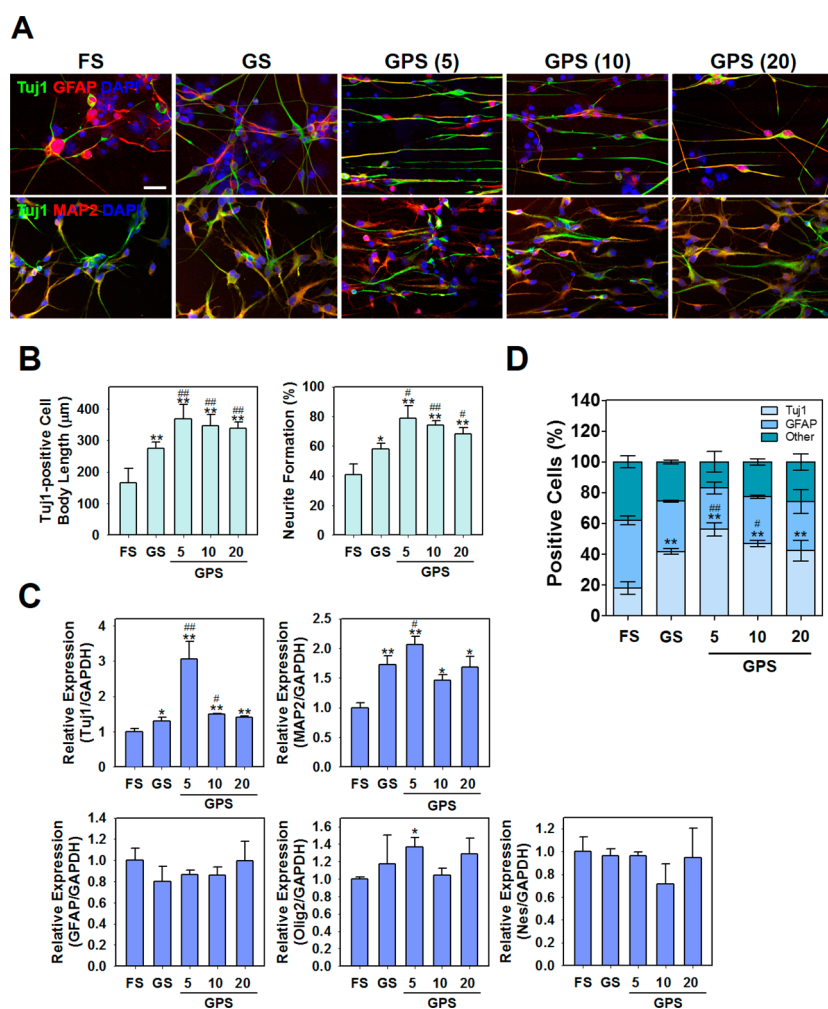


Figure 4. Enhancement of neuronal differentiation of hNSCs on the GPS after 5 days in culture. (A) Immunofluorescent staining to check for the expression of TuJ1 and MAP2 (neuronal markers) and GFAP (astrocyte marker) in hNSCs cultured on each substrate (scale bar = 50 μm). (B) Neurite formation ($n = 3$) and cell body length ($n = 10$) quantified from the TuJ1-stained images ($*p < 0.05$, $**p < 0.01$ versus the FS group; $\#p < 0.05$, $\#\#p < 0.01$ versus the GS group). (C) qRT-PCR analysis to examine the gene expression levels of TuJ1, MAP2, GFAP, Olig2, and Nestin in hNSCs grown on the substrates ($n = 3$; $*p < 0.05$, $**p < 0.01$ versus the FS group; $\#p < 0.05$, $\#\#p < 0.01$ versus the GS group). (D) Relative proportions of TuJ1-positive cells and GFAP-positive cells in total populations of differentiated hNSCs on the substrates ($n = 3$; $*p < 0.05$, $**p < 0.01$ versus the FS group; $\#p < 0.05$, $\#\#p < 0.01$ versus the GS group).

analysis showed that phosphorylation of FAK at Y397 was highly increased in cells cultured on the GPS with a 5 μm groove width compared with that of cells on the other substrates (Figure 3D). In addition, the expression of phosphorylated paxillin (at Y118), which interacts with FAK and recruits it into focal adhesion sites,³⁷ was greatly upregulated in hNSCs cultured on the GPS with a 5 μm groove width (Figure 3D). These data may indicate that the hierarchical structures of the GPS further increase focal adhesion formation and activate FAK-derived signal cascades in the hNSCs by providing combined topographical stimulations capable of promoting both integrin clustering and F-actin alignment. Enhanced integrin clustering and F-actin alignment by GO-based hierarchical topographies may be able to facilitate FAK recruitment to adhesion sites and activate the autophosphorylation of FAK (at Y397), leading to FAK-mediated phosphorylation of paxillin and vinculin associated with paxillin.³⁸ These series of signaling pathways contribute to the maturation of focal adhesion and regulation of the dynamics of cytoskeletal structures, which ultimately affects the differentiation of stem cells.^{39,40}

3.3. Enhanced Neuronal Differentiation of hNSCs by Hierarchical GO Topography.

Next, we investigated whether focal adhesion development and FAK signal activation induced by hierarchical GO topographies really lead to an enhancement in the neuronal differentiation of hNSCs. To verify this hypothesis, hNSCs on the substrates were maintained under culture conditions without any mitogenic factors (bFGF and LIF) for inducing spontaneous differentiation. Immunofluorescent staining for neuronal markers (TuJ1 and MAP2) indicated highly elongated morphology along the GO micro-groove/ridge patterns on the GPS (Figure 4A). The GPS, especially the one with a 5 μm groove width, significantly promoted the neuronal differentiation of hNSCs in comparison to FS and GS. Moreover, hNSCs differentiated on the GPS had a TuJ1-positive body length much greater than that of the cells on the FS and GS (Figure 4B). hNSCs grown on the GPS with a 5 μm groove width also exhibited the most extensive neurite formation (Figure 4B). These results indicate that the GO-based hierarchical topography could enhance neurite formation and outgrowth in hNSCs during neuronal differentiation.

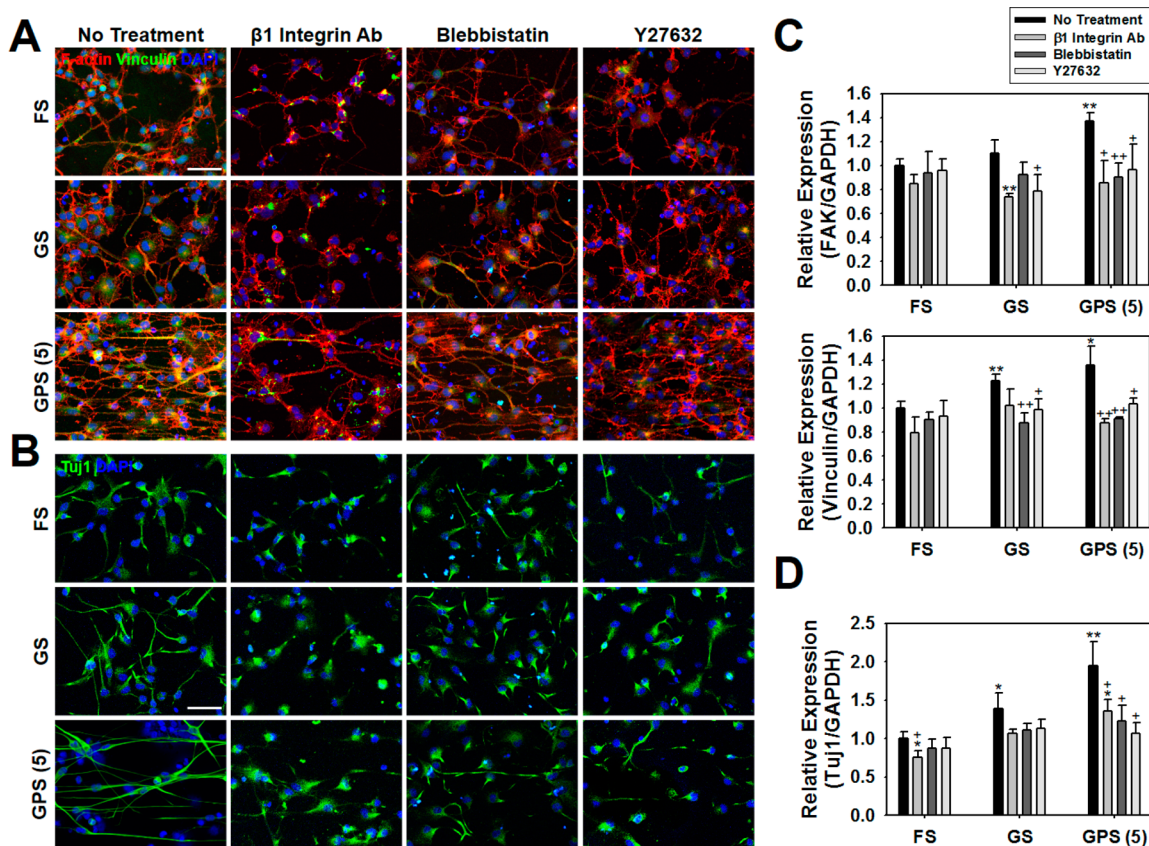


Figure 5. Inhibition of focal adhesion, alignment, and differentiation of hNSCs upon treatment with $\beta 1$ integrin antibodies, blebbistatin (myosin II inhibitor), and Y27632 (ROCK inhibitor) after 1 day in culture. (A) Co-staining of vinculin (focal adhesion protein) and F-actin (cytoskeleton) and (B) immunofluorescent staining of neuronal differentiation marker (Tuj1) in hNSCs on the substrates in the presence or absence of treatments with $\beta 1$ integrin antibodies, blebbistatin, and Y27632 (scale bars = 50 μm). qRT-PCR analysis results quantifying the expression of (C) FAK and vinculin (focal adhesion proteins) and (D) Tuj1 (neuronal marker) in hNSCs on the substrates with or without treatments of $\beta 1$ integrin antibodies, blebbistatin, and Y27632 (* $p < 0.05$, ** $p < 0.01$ versus the untreated FS group; + $p < 0.05$, ++ $p < 0.01$ versus the untreated group for each substrate).

Interestingly, the GPS shifted the propensity of hNSC differentiation toward the neuronal lineage during spontaneous differentiation. qRT-PCR analysis revealed that neuronal (Tuj1 and MAP2) gene expression was highly increased in hNSCs on the GPS with a 5 μm groove width compared to cells cultured on the FS, GS, and other GPS substrates (10 μm and 20 μm groove widths) (Figure 4C), indicating that hierarchical topographies of specific dimensions on the GPS resulted in enhanced differentiation of hNSCs into the neuronal lineage. In contrast, no significant difference was observed in the expression of astrocyte (GFAP) and undifferentiated NSC (nestin) markers among the groups (Figure 4C). Expression of the oligodendrocyte lineage marker (Olig2) was slightly upregulated in hNSCs cultured on the GPS with a 5 μm groove width (Figure 4C). These results may indicate that GPS facilitated lineage specification of hNSCs toward neuronal lineage but did not affect the self-renewal capacity and astrocyte differentiation of hNSCs. Quantification of the relative ratio of the neuronal lineage to other lineages (e.g., astrocytes) confirmed that the Tuj1-positive cell population increased on the GPS with a 5 μm groove width, whereas the GFAP-positive cell population simultaneously decreased on the GPS with a 5 μm groove width (Figure 4D), indicating again that the GPS directs the fate of differentiated hNSCs toward neuronal lineage rather than astrocyte lineage.

3.4. Mechanisms of Enhanced Differentiation of hNSCs by Hierarchical GO Topography.

Several critical

cellular events and pathways involved in mechanotransduction signaling were examined as potential mechanisms of promoted focal adhesion development and differentiation of hNSCs by the hierarchical GO topographical cues containing both nanoroughness and microgroove patterns. Because mechanotransduction signaling is usually initiated from integrin-mediated binding to the substrate, integrin binding and clustering are critical for control of a variety of cellular behaviors, including adhesion, proliferation, and differentiation.⁴¹ In particular, $\beta 1$ integrin interacting with FN is known to play a major role in roughness recognition on graphitic carbon-coated substrates.⁴² In this study, GPS was coated with FN to increase hNSC adhesion, and thus we first targeted the integrin-mediated binding of hNSCs onto FN-coated GO substrates as an initial point for activation of the FAK pathway. Blocking $\beta 1$ integrin-mediated binding of hNSCs by treating $\beta 1$ integrin antibodies significantly inhibited the adhesion and alignment of cells along the microgroove patterned structures, abolishing the effect of the GPS with a 5 μm groove on enhanced focal adhesion development (Figure 5A) and consequently reducing hNSC differentiation into the neuronal lineage (Figure 5B). These results may reflect that $\beta 1$ integrin binding and clustering of hNSCs promoted by GO nanoroughness in the GPS are essential for enhanced focal adhesion development and neuronal differentiation in hNSCs.

Cytoskeleton organization and alignment by the microgroove patterns of the GPS may also be important processes to explain

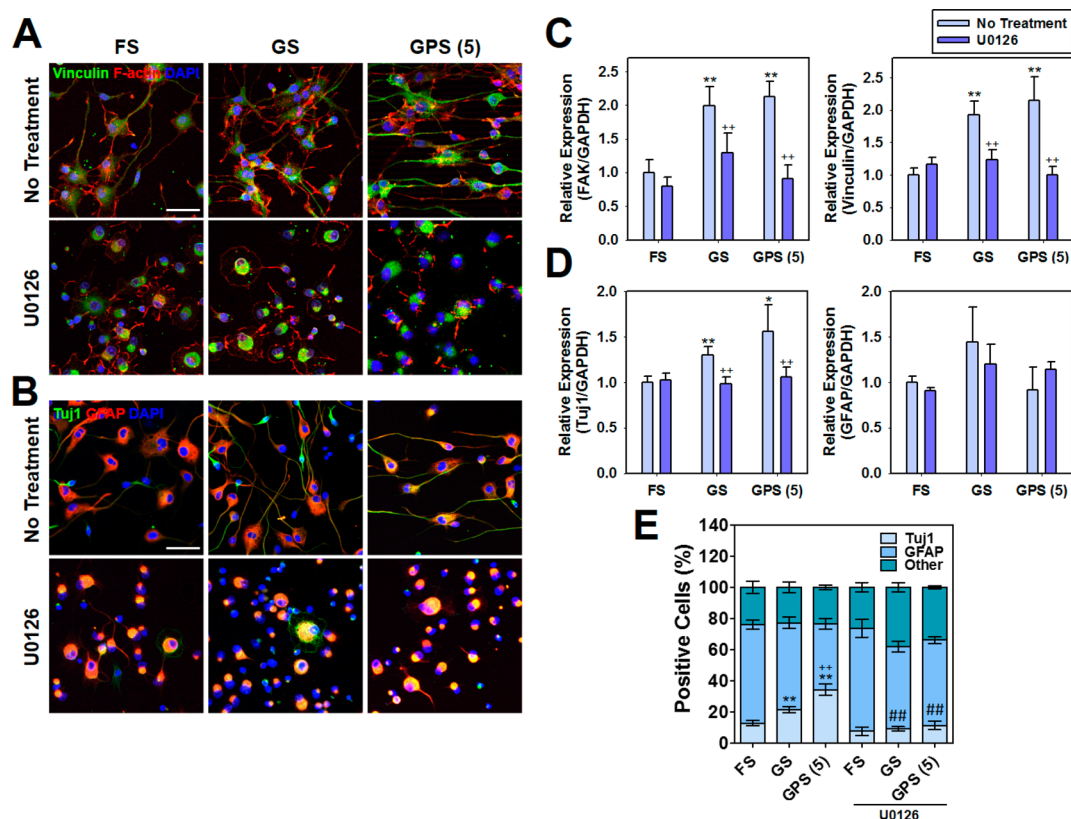


Figure 6. Inhibition of focal adhesion, alignment, and differentiation of hNSCs upon treatment with U0126 (ERK1/2 inhibitor) after 1 day in culture. (A) Co-staining of vinculin (focal adhesion protein) and F-actin (cytoskeleton) and (B) immunofluorescent staining of Tuj1 (neuronal marker) and GFAP (astrocyte marker) of hNSCs on the substrates in the presence or absence of treatment with U0126 (scale bars = 50 μ m). qRT-PCR analysis results quantifying gene expression of (C) FAK and vinculin (focal adhesion proteins) and (D) Tuj1 and GFAP (differentiation markers) in hNSCs with or without treatment of U0126 (* p < 0.05, ** p < 0.01 versus nontreated FS group, ++ p < 0.01 versus no treatment in each substrate group). (E) Relative proportion of Tuj1- and GFAP-positive cells in total populations of differentiated hNSCs with or without treatment of U0126 on each substrate (n = 3, ** p < 0.01 versus Tuj1-positive cells in the nontreated FS group, ++ p < 0.01 versus Tuj1-positive cells in nontreated GS group, ### p < 0.01 versus Tuj1-positive cells in each substrate group without U0126 treatment).

the enhanced neuronal differentiation of hNSCs by hierarchical GO patterns. Thus, hNSCs seeded onto the substrates were treated with two inhibitors of cytoskeleton organization, blebbistatin (myosin II inhibitor) and Y27632 (ROCK pathway inhibitor). Treatment with blebbistatin and Y27632 interrupted hNSC alignment, reduced focal adhesion (Figure 5A), and significantly decreased neuronal differentiation of hNSCs (Figure 5B). qRT-PCR analysis for FAK and vinculin revealed that the gene expression levels of those focal adhesion proteins in hNSCs grown on the GPS with a 5 μ m groove width were remarkably downregulated by the treatments with β 1 integrin antibodies, blebbistatin, and Y27632 compared to those with no treatment (Figure 5C). Accordingly, the gene expression of Tuj1 in hNSCs on the GPS was greatly reduced by the treatments of β 1 integrin antibodies, blebbistatin, and Y27632 (Figure 5D), indicating that cytoskeleton organization, alignment, and the ROCK pathway in hNSCs are critical events for the promoted neuronal differentiation of hNSCs on the GPS.

Enhancement of neuronal differentiation of hNSCs by hierarchical GO topographies may also be due to the activation of downstream signal cascades associated with differentiation following a series of events, including integrin clustering, cytoskeletal rearrangement, focal adhesion assembly, and FAK signal activation.²⁵ Our previous study demonstrated that topographical stimulation-induced mechanotransduction in hNSCs can upregulate gene expression associated with the

differentiation of hNSCs via signaling pathways such as MEK-ERK,²⁵ suggesting that this pathway may also be involved in the enhancement of neuronal differentiation by hierarchical GO topographies in the present study. Thus, we examined whether the MEK-ERK pathway is really associated with enhanced neuronal differentiation of hNSCs by the GPS. To conduct an inhibition assay of the MEK-ERK pathway, hNSCs on the substrates were treated with a MEK-ERK pathway inhibitor (U0126).^{25,43,44} The treatment of U0126 disrupted cytoskeletal alignment, elongation, and neurite extension of hNSCs along the groove patterns on the GPS (Figures 6A and B). The expression of focal adhesion proteins (FAK and vinculin) and a neuronal marker (Tuj1) in hNSCs on the GPS were significantly downregulated by the treatment of U0126 (Figures 6C and D). Interestingly, no significant difference was observed in the expression of an astrocyte marker (GFAP) between nontreated and U0126-treated cells (Figure 6D). The quantification of the relative percentage ratio of neuronal lineage cells (Tuj1-positive cells) and astrocyte lineage cells (GFAP-positive cells) indicated that the elevated level of hNSC differentiation into neuronal lineage on the GPS was completely reversed by U0126 treatment (Figure 6E), suggesting that the MEK-ERK pathway may be responsible for directing hNSC differentiation toward neuronal lineage rather than astrocyte lineage on the GPS. Overall, our results indicate that the MEK-ERK pathway may be involved in the

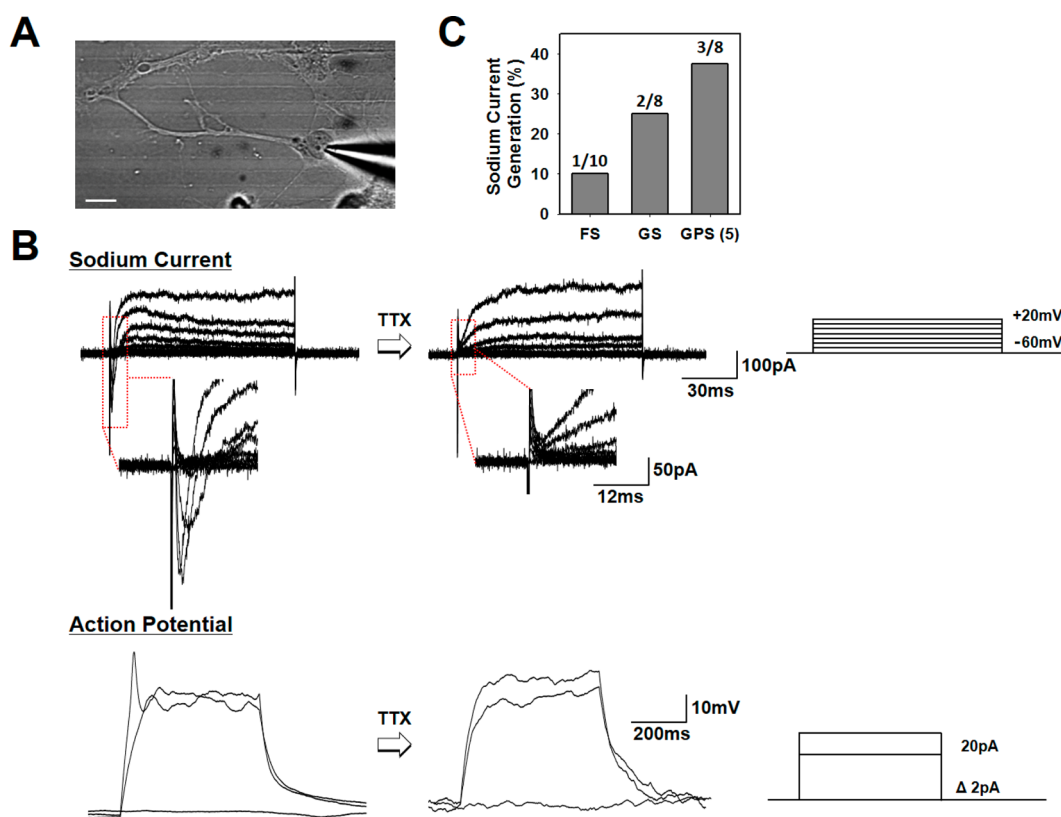


Figure 7. Electrophysiological analysis of differentiated hNSCs on the GPS with 5 μm microgroove patterns for 5 days. (A) Whole-cell patch clamp analysis results measuring sodium channel-mediated currents and action potentials of hNSCs grown on the GPS with 5 μm microgroove patterns. (B) Recording of sodium currents in neuronal lineage cells derived from hNSCs on the GPS with 5 μm microgroove patterns (left). Electrical stimulation from -60 mV to 20 mV was applied to the patched cells (right). The currents were completely eliminated after treatment with 0.5 μM TTX, a sodium-channel blocker (middle). Red boxes show more clearly the presence of transient inward currents before TTX treatment and disappearance of the currents after TTX treatment. The generation of action potential spikes was observed in response to depolarizing current injections (left). Membrane potential was maintained at about -60 mV (right). The action potential spikes disappeared upon treatment with TTX (middle). (C) Comparison of the percentage of cell populations generating sodium currents on different substrates ($n = 8-10$).

enhanced focal adhesion and neuronal differentiation of hNSCs by the GPS, which is consistent with the findings from several previous studies demonstrating that the MEK-ERK pathway is associated with topography-mediated mechanotransduction signal cascades for promoting stem cell differentiation.^{25,43,44}

We also investigated whether treatments of the inhibitors cause a change in other cellular properties in addition to adhesion, alignment, and differentiation. As one such cellular property, we compared the proliferation of hNSCs grown on different substrates (FS, GS, and GPS) using an MTT assay after treatments with $\beta 1$ integrin antibodies and three inhibitors (Y27632, blebbistatin, and U0126). The results obtained from the MTT assay indicated that the mitochondrial metabolic activity of hNSCs treated with these inhibitors on each substrate was not significantly different from that of the hNSCs without inhibitor treatments (Figure S2). This might be because of the optimized doses of each inhibitor that do not affect cell viability while abolishing the effects of substrate topography.^{25,40,43} Therefore, we conclude that treatments of these inhibitors reversed the enhancement in focal adhesion, cytoskeleton alignment, and differentiation of hNSCs by the surface topography of the GPS but did not affect the viability and proliferation of the cells on the substrates. MTT data (Figure S2) also revealed that hNSCs grown on the GPS (no treatment group in GPS) exhibited proliferative capacity similar to that of the cells cultured on other control substrates (no

treatment groups in FS and GS). Thus, these data may indicate that the activation of FAK and ROCK pathways in hNSCs by surface topographies of the GPS did not lead to uncontrolled cell growth.

Graphene-based materials have also been known to influence cellular behaviors such as adhesion and differentiation due to their inherent electrical or physicochemical properties.^{12,17} Previous studies have shown that GO may be able to alter stem cell differentiation patterns due to protein adsorption from the culture medium onto the graphene-coated substrates, changes in surface properties due to graphene coating, or graphene-inherent electrical stimulation, which needs to be further elucidated in future studies.^{14,19,20} In this study, FN was deposited on the GO substrates to improve hNSC adhesion. Nano- and microscale GO surface topographies can influence FN coating in the contexts of protein density and conformation. Because FN directly regulates cell adhesion and differentiation,^{31,45,46} it is important to investigate whether GO patterned topographies affect FN adsorption onto the substrates and how the alteration in FN adsorption influences hNSC differentiation. Thus, we compared the adsorption of FN on each substrate (FS, GS, and GPS) and confirmed that the amount of adsorbed FN was greater ($p < 0.05$) on the GO substrates (GS and 5 μm GPS) than on the FS without GO coating and surface topographies (Figure S3). This indicates that GO could increase FN adsorption onto the substrates.

Interestingly, there was no significant difference in the adsorption of FN between GS and the 5 μm GPS groups (Figure S3). Because GS enhanced neuronal differentiation of hNSCs compared to that of FS (Figure 4), we guess that the increase in FN adsorption by the presence of GO enhanced differentiation of hNSCs into neuronal lineage on the substrates. The data presented in Figure 4 also revealed that GPS was more effective for promoting neuronal differentiation of hNSCs than GS without hierarchical patterned structures. When a similar level of the adsorption of FN on the GS and GPS groups is considered (Figure S3), the promoted neuronal differentiation of hNSCs on the GPS might be mainly attributed to the effect of hierarchical surface topographies of the GPS. Together, our results may suggest a potential mechanism of promoted neuronal differentiation of hNSCs on the GPS by a combined effect of GO-mediated control of FN adsorption and surface topographical cues of the GPS.

3.5. Derivation of Electrophysiologically Functional Neuron-like Cells from hNSCs Cultured on GO-based Hierarchical Patterned Substrates. Finally, we performed a whole-cell patch clamp analysis to investigate whether hNSCs differentiated on the GPS are functional neuronal cells that exhibit electrophysiological functionalities (Figure 7A). Neuronal cells derived from hNSCs on the GPS displayed voltage-dependent ionic currents and action potentials which are electrophysiological characteristics specific to functional, mature neurons, as shown in Figure 7B. To confirm the channel subtypes mediating currents and spikes, the cells were treated with sodium channel antagonist TTX. Due to blocking of sodium channels by TTX treatment, sodium currents and action potentials disappeared (Figure 7B), which revealed that voltage-gated sodium channels mediated the currents and spikes in differentiated hNSCs on the GPS. The percentage of firing cells generating sodium current in the analyzed cells was quantified and compared between different substrate groups. The percentage of sodium current-generating cells in the 5 μm GPS group was higher than that in the FS and GS groups (5 μm GPS at 37.5% versus FS at 10% and GS at 25.0%) (Figure 7C), suggesting that GPS could promote induction of electrophysiologically active neuronal lineage cells from hNSCs. Therefore, GPS is expected to serve as an effective culture platform to produce functional stem cell therapeutics that exhibit electrophysiological properties comparable to those of functional, mature neurons.

4. CONCLUSIONS

In summary, GO-based hierarchical topography enhanced hNSC alignment by GO microgroove/nanoridge and integrin clustering due to GO nanoroughness, which resulted in the promotion of focal adhesion development in hNSCs. Accordingly, the hierarchical GO surfaces enhanced hNSC differentiation and also directed lineage specification of hNSCs into electrophysiologically functional neuron-like cells that generate sodium currents and action potential. The enhanced neuronal differentiation of hNSCs by the hierarchical GO topography seems to be associated with mechanotransduction events, including integrin binding/clustering, focal adhesion development, F-actin alignment, and activation of the FAK, ROCK, and MEK-ERK pathways. Our results suggest that GO surfaces with combined nano- and microstructured topographies could be developed into functional substrates or scaffolds to produce stem cell therapeutics with enhanced

neuronal differentiation capacity, which may give rise to various applications in neural tissue engineering and stem cell therapy.

We believe that our current study has novel views of material design and biological outcomes. First, we used GO-based patterned substrates capable of providing biophysical micro-environments with hierarchically patterned topographies and graphene-inherent effects to stem cells, which could further increase the effect of surface topographical stimulation. Second, we revealed that the use of GPS with hierarchically structured topographies could improve electrophysiological functionality of differentiated hNSCs. With the consideration that previous studies have employed mostly topographies with simple patterned structures for stem cell differentiation and have not provided an evaluation of differentiated stem cells in terms of electrophysiological functionality, our current study may have benefits in material design for stem cell differentiation and biological outcomes by topographical stimulation.

■ ASSOCIATED CONTENT

Supporting Information

The Supporting Information is available free of charge on the ACS Publications website at DOI: 10.1021/acsami.6b01804.

Live/Dead staining of cells cultured on the substrates, fibronectin adsorption on the substrates, and viability data of cells treated with inhibitors (PDF)

■ AUTHOR INFORMATION

Corresponding Authors

*E-mail: taeyoon.lee@yonsei.ac.kr.

*E-mail: seungwoocho@yonsei.ac.kr.

Author Contributions

¹K.Y. and J.L. contributed equally to this work.

Notes

The authors declare no competing financial interest.

■ ACKNOWLEDGMENTS

This work was supported by a grant (HI14C1588) from the Korea Health Technology R&D Project funded by the Ministry of Health and Welfare and a grant (2015R1A2A1A15053771) from the National Research Foundation of Korea (NRF), the Ministry of Science, ICT and Future Planning (MSIP), Republic of Korea. This work was supported in part by the Yonsei University Future-Leading Research Initiative of 2015 (Grant 2015-22-0166). This work was also supported by the Priority Research Centers Program (Grant 2009-0093823) through the National Research Foundation of Korea (NRF) funded by the Ministry of Education, Science, and Technology (MEST).

■ REFERENCES

- (1) Geim, A. K.; Novoselov, K. S. The Rise of Graphene. *Nat. Mater.* **2007**, *6*, 183–191.
- (2) Geim, A. K. Graphene: Status and Prospects. *Science* **2009**, *324*, 1530–1534.
- (3) Zhu, Y.; Murali, S.; Cai, W.; Li, X.; Suk, J. W.; Potts, J. R.; Ruoff, R. S. Graphene and Graphene Oxide: Synthesis, Properties, and Applications. *Adv. Mater.* **2010**, *22*, 3906–3924.
- (4) Akhavan, O.; Choobtashani, M.; Ghaderi, E. Protein Degradation and Rna Efflux of Viruses Photocatalyzed by Graphene–Tungsten Oxide Composite under Visible Light Irradiation. *J. Phys. Chem. C* **2012**, *116*, 9653–9659.

- (5) Hu, W.; Peng, C.; Luo, W.; Lv, M.; Li, X.; Li, D.; Huang, Q.; Fan, C. Graphene-Based Antibacterial Paper. *ACS Nano* **2010**, *4*, 4317–4323.
- (6) Jang, H. D.; Kim, S. K.; Chang, H.; Choi, J.-W. 3d Label-Free Prostate Specific Antigen (PSA) Immunosensor Based on Graphene–Gold Composites. *Biosens. Bioelectron.* **2015**, *63*, 546–551.
- (7) Feng, L.; Wu, L.; Qu, X. New Horizons for Diagnostics and Therapeutic Applications of Graphene and Graphene Oxide. *Adv. Mater.* **2013**, *25*, 168–186.
- (8) Liu, Z.; Robinson, J. T.; Sun, X.; Dai, H. Pegylated Nanographene Oxide for Delivery of Water-Insoluble Cancer Drugs. *J. Am. Chem. Soc.* **2008**, *130*, 10876–10877.
- (9) Li, J.; Lyv, Z.; Li, Y.; Liu, H.; Wang, J.; Zhan, W.; Chen, H.; Chen, H.; Li, X. A Theranostic Prodrug Delivery System Based on Pt (IV) Conjugated Nano-Graphene Oxide with Synergistic Effect to Enhance the Therapeutic Efficacy of Pt Drug. *Biomaterials* **2015**, *51*, 12–21.
- (10) Hong, J.; Shah, N. J.; Drake, A. C.; DeMuth, P. C.; Lee, J. B.; Chen, J.; Hammond, P. T. Graphene Multilayers as Gates for Multi-Week Sequential Release of Proteins from Surfaces. *ACS Nano* **2012**, *6*, 81–88.
- (11) Nayak, T. R.; Andersen, H.; Makam, V. S.; Khaw, C.; Bae, S.; Xu, X.; Ee, P.-L. R.; Ahn, J.-H.; Hong, B. H.; Pastorin, G. Graphene for Controlled and Accelerated Osteogenic Differentiation of Human Mesenchymal Stem Cells. *ACS Nano* **2011**, *5*, 4670–4678.
- (12) Lee, W. C.; Lim, C. H. Y.; Shi, H.; Tang, L. A.; Wang, Y.; Lim, C. T.; Loh, K. P. Origin of Enhanced Stem Cell Growth and Differentiation on Graphene and Graphene Oxide. *ACS Nano* **2011**, *5*, 7334–7341.
- (13) Cong, H. P.; Qiu, J. H.; Yu, S. H. Thermoresponsive Poly (N-Isopropylacrylamide)/Graphene/Au Nanocomposite Hydrogel for Water Treatment by a Laser-Assisted Approach. *Small* **2015**, *11*, 1165–1170.
- (14) Park, J.; Kim, Y. S.; Ryu, S.; Kang, W. S.; Park, S.; Han, J.; Jeong, H. C.; Hong, B. H.; Ahn, Y.; Kim, B. S. Graphene Potentiates the Myocardial Repair Efficacy of Mesenchymal Stem Cells by Stimulating the Expression of Angiogenic Growth Factors and Gap Junction Protein. *Adv. Funct. Mater.* **2015**, *25*, 2590–2600.
- (15) Park, J.; Kim, I. Y.; Patel, M.; Moon, H. J.; Hwang, S. J.; Jeong, B. 2D and 3D Hybrid Systems for Enhancement of Chondrogenic Differentiation of Tonsil-derived Mesenchymal Stem Cells. *Adv. Funct. Mater.* **2015**, *25*, 2573–2582.
- (16) Akhavan, O.; Ghaderi, E.; Abouei, E.; Hatamie, S.; Ghasemi, E. Accelerated Differentiation of Neural Stem Cells into Neurons on Ginseng-Reduced Graphene Oxide Sheets. *Carbon* **2014**, *66*, 395–406.
- (17) Solanki, A.; Chueng, S. T. D.; Yin, P. T.; Kappera, R.; Chhowalla, M.; Lee, K. B. Axonal Alignment and Enhanced Neuronal Differentiation of Neural Stem Cells on Graphene-Nanoparticle Hybrid Structures. *Adv. Mater.* **2013**, *25*, 5477–5482.
- (18) Some, S.; Ho, S.-M.; Dua, P.; Hwang, E.; Shin, Y. H.; Yoo, H.; Kang, J.-S.; Lee, D.-k.; Lee, H. Dual Functions of Highly Potent Graphene Derivative–Poly-L-Lysine Composites to Inhibit Bacteria and Support Human Cells. *ACS Nano* **2012**, *6*, 7151–7161.
- (19) Kim, T.-H.; Shah, S.; Yang, L.; Yin, P. T.; Hossain, M. K.; Conley, B.; Choi, J.-W.; Lee, K.-B. Controlling Differentiation of Adipose-Derived Stem Cells Using Combinatorial Graphene Hybrid-Pattern Arrays. *ACS Nano* **2015**, *9*, 3780–3790.
- (20) Park, S. Y.; Park, J.; Sim, S. H.; Sung, M. G.; Kim, K. S.; Hong, B. H.; Hong, S. Enhanced Differentiation of Human Neural Stem Cells into Neurons on Graphene. *Adv. Mater.* **2011**, *23*, H263–H267.
- (21) Yang, J.; McNamara, L. E.; Gadegaard, N.; Alakpa, E. V.; Burgess, K. V.; Meek, R. D.; Dalby, M. J. Nanotopographical Induction of Osteogenesis through Adhesion, Bone Morphogenic Protein Cosignaling, and Regulation of Micromas. *ACS Nano* **2014**, *8*, 9941–9953.
- (22) McMurray, R. J.; Gadegaard, N.; Tsimbouri, P. M.; Burgess, K. V.; McNamara, L. E.; Tare, R.; Murawski, K.; Kingham, E.; Oreffo, R. O.; Dalby, M. J. Nanoscale Surfaces for the Long-Term Maintenance of Mesenchymal Stem Cell Phenotype and Multipotency. *Nat. Mater.* **2011**, *10*, 637–644.
- (23) Dalby, M. J.; Gadegaard, N.; Tare, R.; Andar, A.; Riehle, M. O.; Herzyk, P.; Wilkinson, C. D.; Oreffo, R. O. The Control of Human Mesenchymal Cell Differentiation Using Nanoscale Symmetry and Disorder. *Nat. Mater.* **2007**, *6*, 997–1003.
- (24) Dalby, M. J.; Gadegaard, N.; Oreffo, R. O. Harnessing Nanotopography and Integrin-Matrix Interactions to Influence Stem Cell Fate. *Nat. Mater.* **2014**, *13*, 558–569.
- (25) Yang, K.; Jung, K.; Ko, E.; Kim, J.; Park, K. I.; Kim, J.; Cho, S.-W. Nanotopographical Manipulation of Focal Adhesion Formation for Enhanced Differentiation of Human Neural Stem Cells. *ACS Appl. Mater. Interfaces* **2013**, *5*, 10529–10540.
- (26) Yang, K.; Jung, H.; Lee, H.-R.; Lee, J. S.; Kim, S. R.; Song, K. Y.; Cheong, E.; Bang, J.; Im, S. G.; Cho, S.-W. Multiscale, Hierarchically Patterned Topography for Directing Human Neural Stem Cells into Functional Neurons. *ACS Nano* **2014**, *8*, 7809–7822.
- (27) Pan, Z.; Yan, C.; Peng, R.; Zhao, Y.; He, Y.; Ding, J. Control of Cell Nucleus Shapes via Micropillar Patterns. *Biomaterials* **2012**, *33*, 1730–1735.
- (28) Bettinger, C. J.; Langer, R.; Borenstein, J. T. Engineering Substrate Topography at the Micro- and Nanoscale to Control Cell Function. *Angew. Chem., Int. Ed.* **2009**, *48*, 5406–5415.
- (29) Li, N.; Zhang, Q.; Gao, S.; Song, Q.; Huang, R.; Wang, L.; Liu, L.; Dai, J.; Tang, M.; Cheng, G. Three-Dimensional Graphene Foam as a Biocompatible and Conductive Scaffold for Neural Stem Cells. *Sci. Rep.* **2013**, *3*, 1604.
- (30) Yang, K.; Park, H.-J.; Han, S.; Lee, J.; Ko, E.; Kim, J.; Lee, J. S.; Yu, J. H.; Song, K. Y.; Cheong, E. Recapitulation of in Vivo-Like Paracrine Signals of Human Mesenchymal Stem Cells for Functional Neuronal Differentiation of Human Neural Stem Cells in a 3D Microfluidic System. *Biomaterials* **2015**, *63*, 177–188.
- (31) Yang, K.; Han, S.; Shin, Y.; Ko, E.; Kim, J.; Park, K. I.; Chung, S.; Cho, S.-W. A Microfluidic Array for Quantitative Analysis of Human Neural Stem Cell Self-Renewal and Differentiation in Three-Dimensional Hypoxic Microenvironment. *Biomaterials* **2013**, *34*, 6607–6614.
- (32) Yang, K.; Lee, J. S.; Kim, J.; Lee, Y. B.; Shin, H.; Um, S. H.; Kim, J. B.; Park, K. I.; Lee, H.; Cho, S.-W. Polydopamine-Mediated Surface Modification of Scaffold Materials for Human Neural Stem Cell Engineering. *Biomaterials* **2012**, *33*, 6952–6964.
- (33) Yang, K.; Park, E.; Lee, J. S.; Kim, I. S.; Hong, K.; Park, K. I.; Cho, S.-W.; Yang, H. S. Biodegradable Nanotopography Combined with Neurotrophic Signals Enhances Contact Guidance and Neuronal Differentiation of Human Neural Stem Cells. *Macromol. Biosci.* **2015**, *15*, 1348–1356.
- (34) Park, H.-J.; Yang, K.; Kim, M.-J.; Jang, J.; Lee, M.; Kim, D.-W.; Lee, H.; Cho, S.-W. Bio-Inspired Oligovitronectin-Grafted Surface for Enhanced Self-Renewal and Long-Term Maintenance of Human Pluripotent Stem Cells under Feeder-Free Conditions. *Biomaterials* **2015**, *50*, 127–139.
- (35) Akhavan, O.; Ghaderi, E. Differentiation of Human Neural Stem Cells into Neural Networks on Graphene Nanogrids. *J. Mater. Chem. B* **2013**, *1*, 6291–6301.
- (36) Shi, X.; Chang, H.; Chen, S.; Lai, C.; Khademhosseini, A.; Wu, H. Regulating Cellular Behavior on Few-Layer Reduced Graphene Oxide Films with Well-Controlled Reduction States. *Adv. Funct. Mater.* **2012**, *22*, 751–759.
- (37) Zaidel-Bar, R.; Milo, R.; Kam, Z.; Geiger, B. A Paxillin Tyrosine Phosphorylation Switch Regulates the Assembly and Form of Cell-Matrix Adhesions. *J. Cell Sci.* **2006**, *120*, 137–148.
- (38) Pasapera, A. M.; Schneider, I. C.; Rericha, E.; Schlaepfer, D. D.; Waterman, C. M. Myosin II Activity Regulates Vinculin Recruitment to Focal Adhesions through Fak-Mediated Paxillin Phosphorylation. *J. Cell Biol.* **2010**, *188*, 877–890.
- (39) Turner, C. E. Paxillin and Focal Adhesion Signalling. *Nat. Cell Biol.* **2000**, *2*, E231–E236.
- (40) Teo, B. K. K.; Wong, S. T.; Lim, C. K.; Kung, T. Y.; Yap, C. H.; Ramagopal, Y.; Romer, L. H.; Yim, E. K. Nanotopography Modulates Mechanotransduction of Stem Cells and Induces Differentiation through Focal Adhesion Kinase. *ACS Nano* **2013**, *7*, 4785–4798.

- (41) Hynes, R. O. Integrins: Versatility, Modulation, and Signaling in Cell Adhesion. *Cell* **1992**, *69*, 11–25.
- (42) Olivares-Navarrete, R.; Rodil, S. E.; Hyzy, S. L.; Dunn, G. R.; Almaguer-Flores, A.; Schwartz, Z.; Boyan, B. D. Role of Integrin Subunits in Mesenchymal Stem Cell Differentiation and Osteoblast Maturation on Graphitic Carbon-Coated Microstructured Surfaces. *Biomaterials* **2015**, *51*, 69–79.
- (43) Chen, Y.-C.; Lee, D.-C.; Tsai, T.-Y.; Hsiao, C.-Y.; Liu, J.-W.; Kao, C.-Y.; Lin, H.-K.; Chen, H.-C.; Palathinkal, T. J.; Pong, W.-F. Induction and Regulation of Differentiation in Neural Stem Cells on Ultra-Nanocrystalline Diamond Films. *Biomaterials* **2010**, *31*, 5575–5587.
- (44) Mruthyunjaya, S.; Manchanda, R.; Godbole, R.; Pujari, R.; Shiras, A.; Shastry, P. Laminin-1 Induces Neurite Outgrowth in Human Mesenchymal Stem Cells in Serum/Differentiation Factors-Free Conditions through Activation of FAK–MEK/ERK Signaling Pathways. *Biochem. Biophys. Res. Commun.* **2010**, *391*, 43–48.
- (45) Martino, M. M.; Mochizuki, M.; Rothenfluh, D. A.; Rempel, S. A.; Hubbell, J. A.; Barker, T. H. Controlling Integrin Specificity and Stem Cell Differentiation in 2D and Environments through Regulation of Fibronectin Domain Stability. *Biomaterials* **2009**, *30*, 1089–1097.
- (46) Yang, F.; Cho, S.-W.; Son, S. M.; Hudson, S. P.; Bogatyrev, S.; Keung, L.; Kohane, D. S.; Langer, R.; Anderson, D. G. Combinatorial Extracellular Matrices for Human Embryonic Stem Cell Differentiation in 3D. *Biomacromolecules* **2010**, *11*, 1909–1914.